Computer Methods and Programs in Biomedicine 219 (2022) 106777

Contents lists available at ScienceDirect

Computer Methods and Programs in Biomedicine

journal homepage: www.elsevier.com/locate/cmpb

Differential evolution method to find optimal location of a single-element transducer for transcranial focused ultrasound therapy

Tae Young Park[a,b], Hyo-Jin Kim[c], So Hui Park[d], Won Seok Chang[d], Hyungmin Kim[a,b,*], Kyungho Yoon[e,**]

[a] Bionics Research Center, Biomedical Research Division, Korea Institute of Science and Technology, Seoul 02792, Republic of Korea
[b] Division of Bio-Medical Science and Technology, KIST School, Korea University of Science and Technology, Seoul 02792, Republic of Korea
[c] Center for Healthcare Robotics, Korea Institute of Science and Technology, Seoul 02792, Republic of Korea
[d] Department of Neurosurgery, Brain Research Institute, Yonsei University College of Medicine, Seoul 04527, Republic of Korea
[e] School of Mathematics and Computing (Computational Science and Engineering), Yonsei University, Seoul 03722, Republic of Korea

ARTICLE INFO

Article history:
Received 14 December 2021
Revised 14 March 2022
Accepted 24 March 2022

Keywords:
Transcranial focused ultrasound
Single-element transducer
Guidance system
Numerical simulation
Optimization
Differential evolution

ABSTRACT

Background and objective: Focused ultrasound (FUS) has been receiving growing attention as a noninvasive brain stimulation tool because of its superior spatial specificity and depth penetrability. However, the large mismatch of acoustic properties between the skull and water can disrupt and shift the acoustic focus in the brain. In this paper, we present a numerical method to find the optimal location of a single-element FUS transducer, which creates focus on the target region.

Methods: The score function, representing the superposition of acoustic waves according to the relative phase difference and transmissibility, was defined based on time-reversal invariance of acoustic waves and depending on the spatial location of the transducer. The optimal location of the transducer was then determined using a differential evolution algorithm. To assess the proposed method, we conducted a forward simulation and compared the resulting focal location to the desired target point. We also performed experimental validation by measuring the acoustic pressure field through an *ex vivo* human skull in a water tank.

Results: The numerical results indicated that the score function had a positive proportional relationship with the acoustic pressure at the target. Moreover, for the optimized transducer location, both the numerical and experimental results showed that the normalized acoustic pressure at the target was higher than 0.9.

Conclusions: In this study, we developed an optimization method to place a single-element transducer that effectively transmits acoustic energy to the targeted region in the brain. Our numerical and experimental results demonstrate that the proposed method can provide an optimal transducer location for safe and efficient FUS treatment.

1. Introduction

Focused ultrasound (FUS), owing to its advantages of excellent spatial selectivity and penetration depth, has garnered increasing attention in the field of noninvasive brain stimulation [1–4]. However, because ultrasound waves are prone to be reflected and refracted by complicated biological tissue structures, there are many significant challenges in the accurate targeting of the FUS focus on a subject-specific target region in the body [5,6]. In particular, in the case of transcranial application of FUS, the presence of the skull intensifies the difficulties, causing various problems such as focal shifting, extra foci, high energy loss, and reverberation [5,6].

The use of a multi-array FUS system helps to compensate for concerns over the skull through individual adjustment of the phase for each ultrasound source element [7]. Using the time-reversal invariance of the ultrasound wave [8,9], time-reversal simulation of the emitting ultrasound at the target point is performed, and the relative phase differences between the target point and each source point are evaluated [7,10]. To maximize the superposition

* Corresponding author at: Bionic Research Center, Korea Institute of Science and Technology, Seoul 02792, Republic of Korea.
** Corresponding author at: School of Mathematics and Computing (Computational Science and Engineering), Yonsei University, Seoul 03722, Republic of Korea.
E-mail addresses: hk@kist.re.kr (T.Y. Park), hk@kist.re.kr (H. Kim), yoonkh@yonsei.ac.kr (K. Yoon).

https://doi.org/10.1016/j.cmpb.2022.106777

of waves, phase tuning was applied to each source element using the relative phase difference. This technique has been successfully demonstrated in animal and human skulls [11–15]. It helps to accurately target during transcranial FUS applications such as thermal ablation [11,12], blood-brain barrier opening [13], and neuromodulation [14,15].

The single-element FUS transducer, owing to its cost-effectiveness and device simplicity, has been widely used instead of the multi-array FUS system [16–19]. To place the invisible focus of a single-element transducer at the target area in the brain, a neuronavigation system via optical tracking has been used as the gold standard [17–22]. The neuronavigation system helps to aim at a target by tracking the relative location of the transducer toward the subject-specific target area. However, such simple geometrical derivation could often be insufficient because the presence of the skull in ultrasound wave propagation may cause significant aberration. To solve this, the 3D-printed holographic lens, which can alleviate skull-induced aberration by the phase correction according to the shape of the lens, has been suggested [23,24]. As another solution, Park et al. proposed a method to find the position of the transducer that minimizes acoustic wave reflection by integrating the reflection coefficients on ultrasound beamlines [25]. However, it could not fully describe the wave propagation through the skull because the ultrasound wave was simplified as straight lines (i.e., beamlines). Moreover, information regarding the optimal orientation of the transducer was not obtained.

In this paper, we propose a numerical optimization method to find the optimal spatial location of the transducer (i.e., position and orientation of the transducer) that creates an acoustic focus on the target region. The aberrations of the wave phase and amplitude induced by the presence of the skull were calculated through a time-reversal simulation of the emitting ultrasound at the target point. The score function, which represents the superposition of acoustic waves according to the relative phase difference and pressure transmissibility, was calculated for the given transducer location. The optimal location of the FUS transducer is determined by maximizing the score function using the differential evolution (DE) optimization method. To assess the performance of the proposed method, we conducted a forward simulation (i.e., forward acoustic propagation from the transducer to the target) using the obtained optimal location of the transducer and compared the resulting focal volume to the target point. We also performed experimental validation by measuring the actual pressure map through the *ex vivo* human skull in a water tank.

2. Material and Methods

2.1. Preparation of human skull images

All data acquisition in this study was performed under the approval of the Institutional Review Board at Yonsei University College of Medicine, Severance Hospital. We acquired computed tomography (CT) image data from four subjects (n = 4, labeled as S1–4) for numerical demonstration and from an ex vivo human skull (n = 1) for experimental validation. The ex vivo human skull was fixed and stored in buffered formalin over ten days. The CT images for numerical models were scanned on a CT scanner (GE Medical Systems, Chicago, US) with a range of 230 × 230 × 159 mm^3 (0.45 × 0. 45 × 0.62 mm^3 resolutions in a 512 × 512 in-plane matrix and 256 slices). For brain anatomy, T1-weighted magnetic resonance imaging (MRI) scanning was also conducted using a 3T scanner (GE medical systems, Chicago, US) with a range of 220 × 220 × 256 mm^3 (0.43 × 0.43 × 1.00 mm^3 resolution, and 512 × 512 in-plane matrix and 256 slices). In addition, the CT images for the ex vivo human skull were acquired using a CT scanner (GE Medical Systems, Chicago, US) with a range of 271 × 271 × 209 mm^3 (0.53 × 0.53 × 0.50 mm^3 resolutions in a 512 × 512 in-plane matrix and 417 slices).

Table 1
Acoustic properties.

Speed of sound (m/s)	Density (kg/m^3)	Attenuation coefficient (Np/MHz/m)
$c_{bone} = 3100$ $c_{water} = 1482$	$\rho_{bone} = 2200$ $\rho_{water} = 1000$	$\alpha_{\min,skull} = 21.5$, $\alpha_{\max,skull} = 208.9$ $\alpha_{water} = 0.025$

2.2. Acoustic simulation

All forward and time-reversal simulations in this study were performed using the k-Wave toolbox [26]. All simulations ended at 100 μs with a Courant–Friedrichs–Lewy (CFL) condition of 0.1. The simulation domain was defined using the preprocessed skull CT images, which were cropped and resampled considering the location of the target point and sonication conditions. The cropped volume was a cube with a size of 189 × 189 × 189 mm^3 (corresponding to 2.3 times the transducer's focal length), where the target point was located at the center of the cropped volume. The windowed-sinc interpolation method [27] was used to resample the cropped volume as iso-voxels of 0.9 mm^3 (i.e., 2π points per wavelength) [5,28]. To describe the porous and inhomogeneous characteristics of the skull, the acoustic properties of the skull model were defined based on the Hounsfield unit (HU) values of the preprocessed CT images. The HU values of CT scans were clipped to a range of [0,3000] with the threshold condition (HU<250 set as 0). Based on the porosity of the skull (P), the acoustic properties were defined using the following equations ((1) – (4)) [5,28]. The skull model was assumed to be immersed in free water. The acoustic properties of the skull and water used are summarized in Table 1 [25,28].

$$P = 1 - \frac{HU}{Max(HU)} \tag{1}$$

$$c_{skull} = c_{water}P + c_{bone}(1 - P) \tag{2}$$

$$\rho_{skull} = \rho_{water}P + \rho_{bone}(1 - P) \tag{3}$$

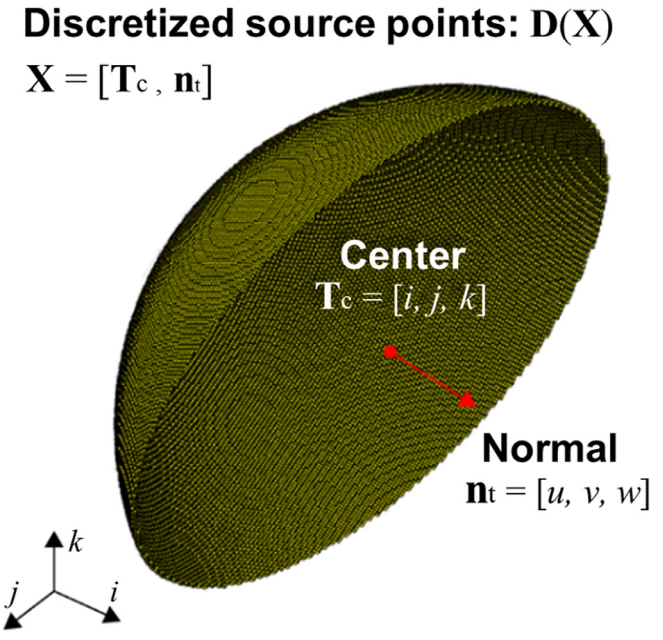

Fig. 1. Discretized source model D(X) of FUS transducer representing source surface of the transducer geometry. The red dot and arrow indicate the transducer center coordinate (T_c) and its normal direction (n_t), respectively.

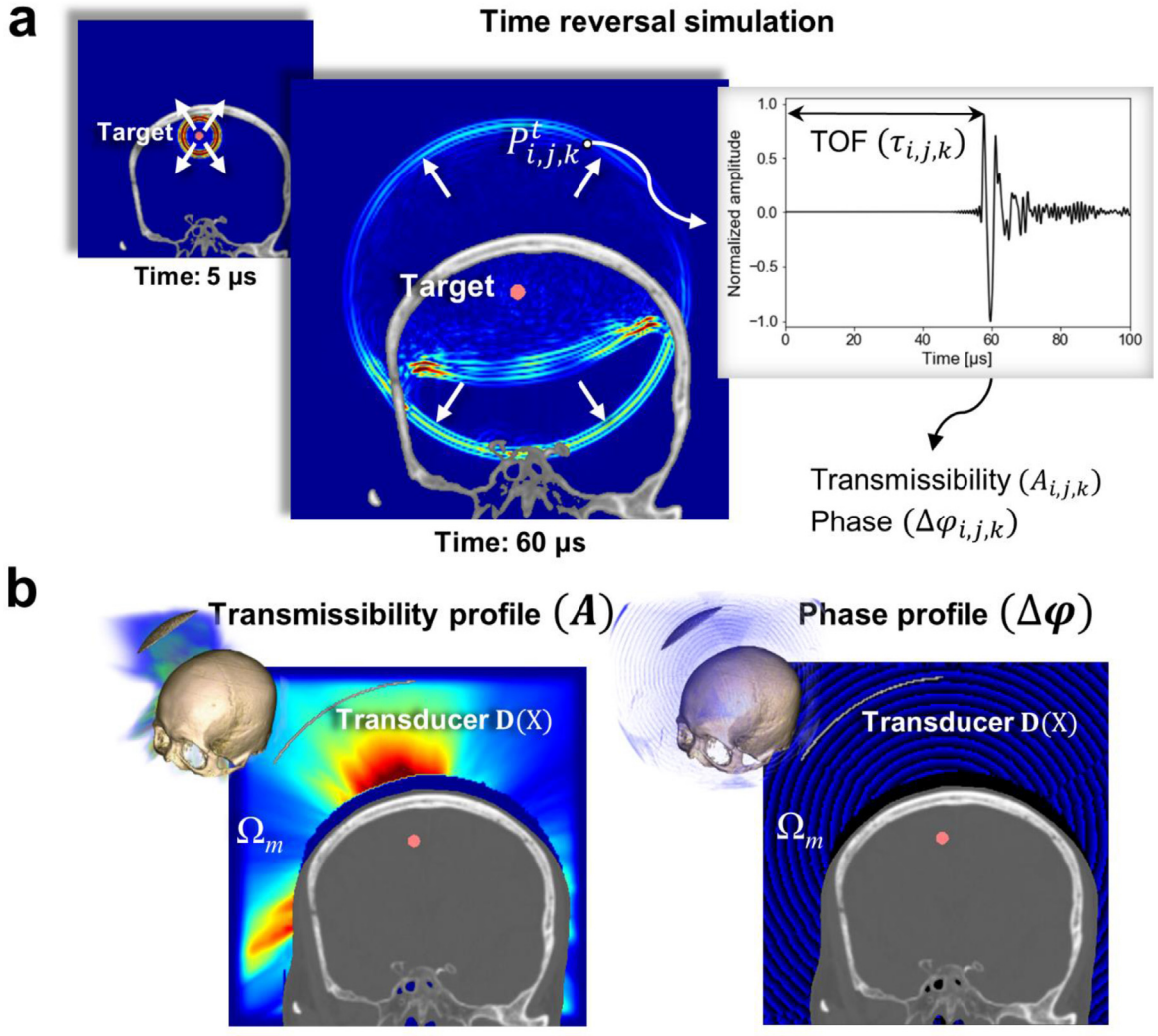

Fig. 2. Schematics of score function evaluation. a) Example of the time-reversal simulation. The ultrasound pulse was emitted from the target point and propagated out of the skull. b) Example of the phase ($\Delta\varphi$) and transmissibility (A) profiles obtained from the arrived pressure signal ($P^t_{i,j,k}$). Ω_m indicates the transducer maneuvering space.

$$\alpha_{skull} = \alpha_{water}P + \left(\alpha_{max,skull} - \alpha_{min,skull}\right)P^{0.5} \quad (4)$$

2.3. Transducer modeling

A single-element FUS transducer (GPS250-D80-FL110, Ultran Group, Hoboken, NJ) operating at 250 kHz was used in this study [29,30]. The transducer consisted of a piezoelectric disc generating ultrasound and a concave-shaped acoustic lens for focusing. The transducer had a diameter of 95 mm, a radius of curvature (ROC) of 99 mm, and a focal length of 85 mm. This transducer was used for the treatment of human Alzheimer's disease [29,30]. The geometry of the concave lens surface was discretized for numerical modeling and used as the ultrasound source points, as shown in Fig. 1. For the given location of the transducer, the transducer location **X** is defined as follows:

$$\mathbf{X} = [\mathbf{T}_c,\ \mathbf{n}_t];\ \mathbf{T}_c = [i, j, k],\ \mathbf{n}_t = [u,\ v,\ w] \quad (5)$$

where $\mathbf{T}_c$ is the center coordinate of the transducer (defined by the central point of the exit plane) represented by the index number (i.e., *i*, *j*, and *k*) in the processed CT image, and $\mathbf{n}_t$ is the normal direction of the exit plane (i.e., the orientation of the transducer) in the 3D Cartesian coordinate system. The discretized source point group is defined as $\mathbf{D}(\mathbf{X})$.

2.4. Time-reversal simulation and evaluation of score function

A time-reversal simulation was performed to obtain the wave phase and transmissibility profiles relative to the desired target point, shown in Fig. 2a. One cycle of a 250 kHz sine wave was emitted at the target point and propagated through the skull. We recorded the arrival pressure wave signal ($P^t_{i,j,k}$) during time t in the space for maneuvering the transducer ($P^t_{i,j,k}$ with $i, j, k \in \Omega_m$), where Ω_m is defined as all voxels of the simulation domain except for the transducer locations in contact with the subject's head (Fig. 2b). The time-of-flight (TOF), $\tau_{i,j,k}$, was defined as the time t when the arrival pressure signal ($P^t_{i,j,k}$) has the maximum value. The phase difference profile ($\Delta\varphi_{i,j,k}$) relative to the target point was evaluated as follows:

$$\Delta\varphi_{i,j,k} = 2\pi\frac{MOD\left(\tau_{i,j,k},\ T\right)}{T} \quad (6)$$

where T is the period of the ultrasound source. *MOD* indicates the modulo operation returning the remainder of a division. The transmissibility profile ($A_{i,j,k}$) is defined by the peak amplitude of the recorded signal ($P^t_{i,j,k}$). The score function (ψ) for the given discretized transducer $\mathbf{D}(\mathbf{X})$ is defined by the phase ($\Delta\varphi_{i,j,k}$) and

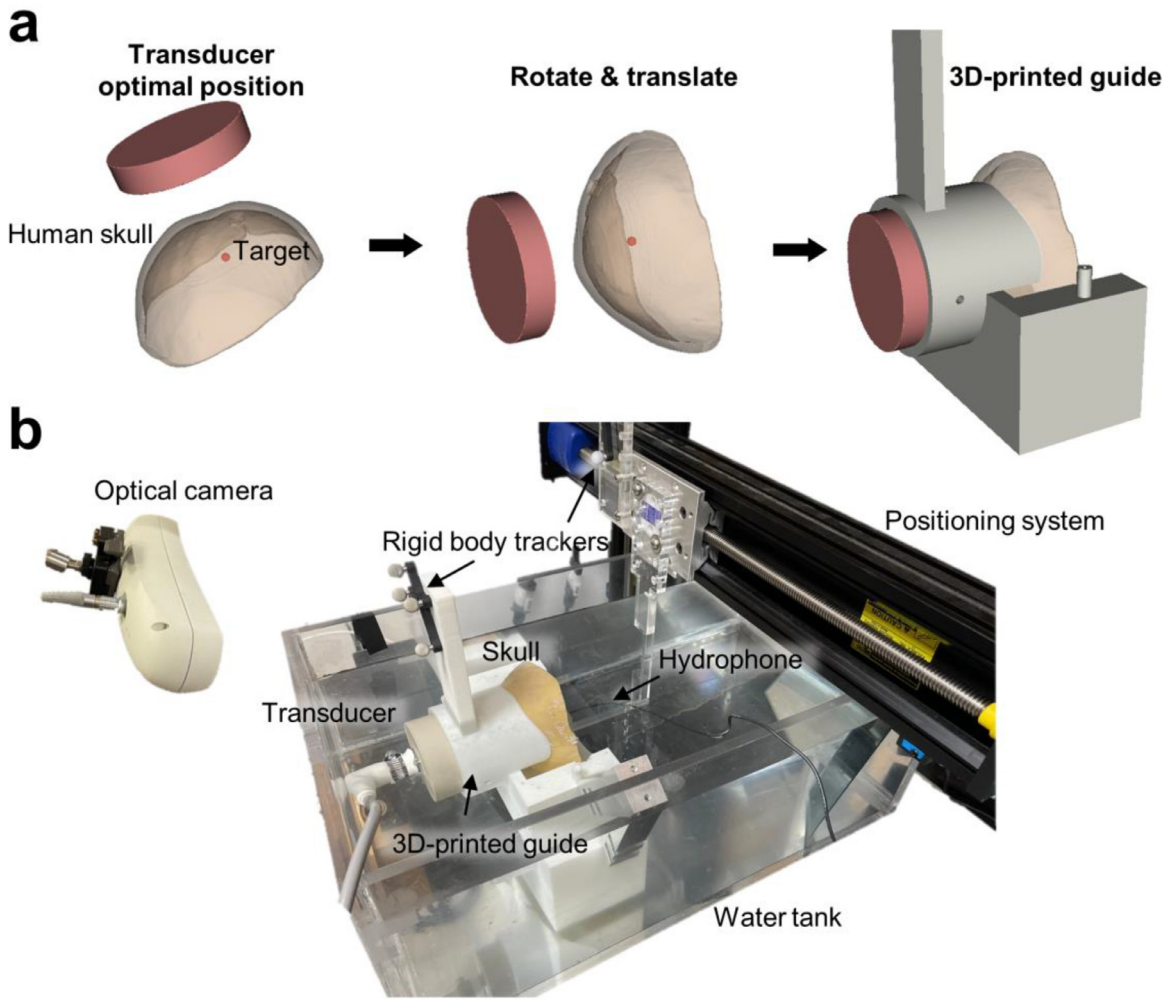

Fig. 3. The experimental setup. a) The process of making a 3D-printed guide. The guide was used to fix the transducer at the optimized location. b) The measurement setup for acquiring acoustic pressure field.

transmissibility ($A_{i,j,k}$) profiles as:

$$\psi(\mathbf{D}(\mathbf{X})) = \left| \sum_{i,j,k \in \mathbf{D}(\mathrm{X})} A_{i,j,k} \exp\left[i\left(\Delta\varphi_{i,j,k}\right)\right] \right| \tag{7}$$

In this study, we hypothesized that the transducer location ($\mathbf{X}$) with the maximal score would be the optimal transducer location.

2.5. Differential evolution optimization

To find the optimal location of the transducer, the DE algorithm [31,32] was utilized with the following constrained optimization problem (p).

$$(p)\ \ maximize\ \ \psi(\mathbf{D}(\mathbf{X})) \tag{8}$$

2.5.1. Population initialization

DE begins by creating an initial population of the target vector, that is, the transducer location ($\mathbf{X}$), denoted by

$$\mathbf{X}_{i,\ \mathrm{G}}\ \ i = 1,\ \ \ldots, NP;\ \ \mathrm{G} = 0, \ldots, \mathrm{G}_{max} \tag{9}$$

where i is the index for the individuals, G indicates the current generation, and NP (=15) [33] is the population size. The initial individuals ($\mathbf{X}_{i,0}$) are randomly selected by the lower and upper bounds of each parameter, as follows:

$$\mathbf{X}_{i,0} = u \cdot (b_U - b_L) + b_L \tag{10}$$

where u is a uniformly distributed random number between 0 and 1, and b_U and b_L denote the lower and upper bounds, respectively. In this study, the bounds were defined under the condition $\mathbf{D}(\mathbf{X}) \in \Omega_m$.

2.5.2. Mutation

For each vector $\mathbf{X}_{i,\mathrm{G}}$ in the population, a mutation operation adding a weight difference between two vectors was used to generate a mutated vector $\mathrm{V}_{i,\mathrm{G}}$ according to the following scheme equation:

$$\mathbf{V}_{i,\ \mathrm{G}} = \mathbf{X}_{\mathrm{best},\ \mathrm{G}} + \mathrm{F} \cdot (\mathbf{X}_{\mathrm{r1},\ \mathrm{G}} - \mathbf{X}_{\mathrm{r2},\ \mathrm{G}}) \tag{11}$$

where the vector indices r1 and r2 are the population indices that are randomly selected. The vector $\mathbf{X}_{\mathrm{best,\ G}}$ is the best solution (i.e., greatest ψ of a generation) for the current generation. The scaling factor F, randomly changed between 0.5 and 1, controls the amplification of the differential variation between the two random vectors, $\mathbf{X}_{\mathrm{r1,\ G}}$ and $\mathbf{X}_{\mathrm{r2,\ G}}$.

2.5.3. Crossover

After the mutation, a crossover operator was applied to $\mathbf{X}_{i,\mathrm{G}}$ and $\mathbf{V}_{i,\mathrm{G}}$ to generate trial vectors $\mathbf{Z}_{i,\mathrm{G}}$. A uniform crossover is employed, and the trial vector is generated by the following equation:

$$\mathbf{Z}_{i,\ \mathrm{G}} = \begin{cases} \mathbf{V}_{i,\ \mathrm{G}}\ if\ u \le C \\ \mathbf{X}_{i,\ \mathrm{G}}\ otherwise \end{cases} \tag{12}$$

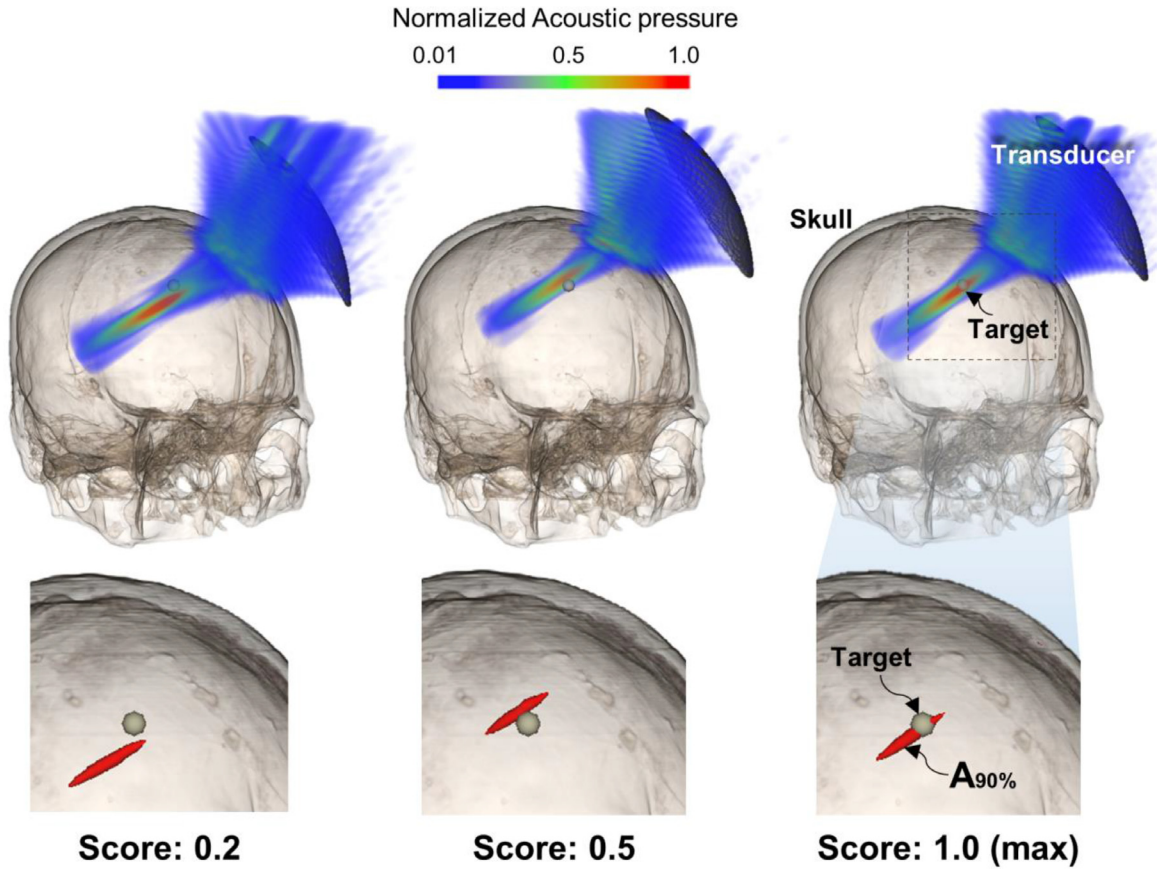

Fig. 4. The first row shows the simulated 3D acoustic pressure distribution depending on a given transducer score. The second row indicates $A_{90\%}$ (red ellipsoid). The gray sphere indicates the stimulation target.

where u is a uniformly distributed number between 0 and 1 (, the same number as in Eq. 10), and C (=0.7) [33] is the crossover probability, which controls the probability of selecting the value in each dimension for a trial vector from a mutated vector.

2.5.4. Selection and stopping criteria

The selection operation, to select the better individual, is achieved from the target and trial vectors by comparing their fitness values through the objective function (i.e., $\psi(\mathbf{D}(\mathbf{X}))$). In the case of maximization problems, the trial vector and the target vector are compared, and the vector with higher $\psi(\mathbf{D}(\mathbf{X}))$ can move to the next generation, as denoted below:

$$\mathbf{X}_{i,\ G+1} = \begin{cases} \mathbf{Z}_{i,\ G} \ if\ \ \psi(\mathbf{D}(\mathrm{Z}_{i,\ G})) \geq \psi(\mathbf{D}(\mathrm{X}_{i,\ G})) \\ \mathbf{X}_{i,\ G} \ otherwise \end{cases} \tag{13}$$

After the selection operation, the optimizer checks whether the population of the new generation satisfies the given stopping criteria.

Optimizer stop when :

$$std(\psi(\mathbf{D}(\mathbf{X}_{G+1}))) \leq t \cdot |mean(\psi(\mathbf{D}(\mathbf{X}_{G+1})))| \tag{14}$$

where t (=0.01) is the relative tolerance for convergence. In this study, the DE algorithm was tested for 3000–5000 transducer locations (denoted as $\mathbf{X}_{total}$) to achieve optimal location. This algorithm was implemented using SciPy 1.7.1, an open-source library for Python [33].

2.6. Numerical validation

To evaluate the performance of the proposed optimization method, forward simulations were conducted with the transducer location ($\mathbf{X}$) used in the DE optimization method. After sorting $\mathbf{X}_{total}$ in descending order of the resulting score value of $\psi(\mathbf{D}(\mathbf{X}))$, 10% of the transducer locations were chosen through a systematic sampling method [34]. Using the intracranial acoustic pressure distribution obtained from the forward simulation, we assessed the relationship between the score value and the spatial conformity of the acoustic focus. The volume of the acoustic focus was defined as the 90%-maximum of intracranial acoustic pressure (denoted as $A_{90\%}$) [28,35], since the previous studies [36,37] have reported that the ultrasound-induced neuromodulatory effects appear within $A_{90\%}$. For comparison, the obtained acoustic simulation results were normalized by the largest value of P_{peak} (i.e., peak intracranial pressure) among all transducer locations. To evaluate the spatial conformity of the acoustic focus, (i) acoustic pressure at the target point (denoted as P_{target}) and (ii) the distance between the target and the $A_{90\%}$ (denoted as Δd) were obtained for the given transducer location. Δd was assigned as 0 mm when the target was in the $A_{90\%}$. For the target out of the $A_{90\%}$, Δd was defined as the shortest distance between the target and the $A_{90\%}$.

To assess our method at various target locations, the evaluation was performed with four brain targets across four subjects, the primary motor cortex (M1), primary visual cortex (V1), dorsal anterior cingulate cortex (dACC), and thalamus. Through co-registration of the ICBM152 template [38] and the T1-weighted images of each subject using the 'Elastix' module in 3D Slicer [39], the four brain target points with subject-specific coordinates for each skull CT data were obtained [28].

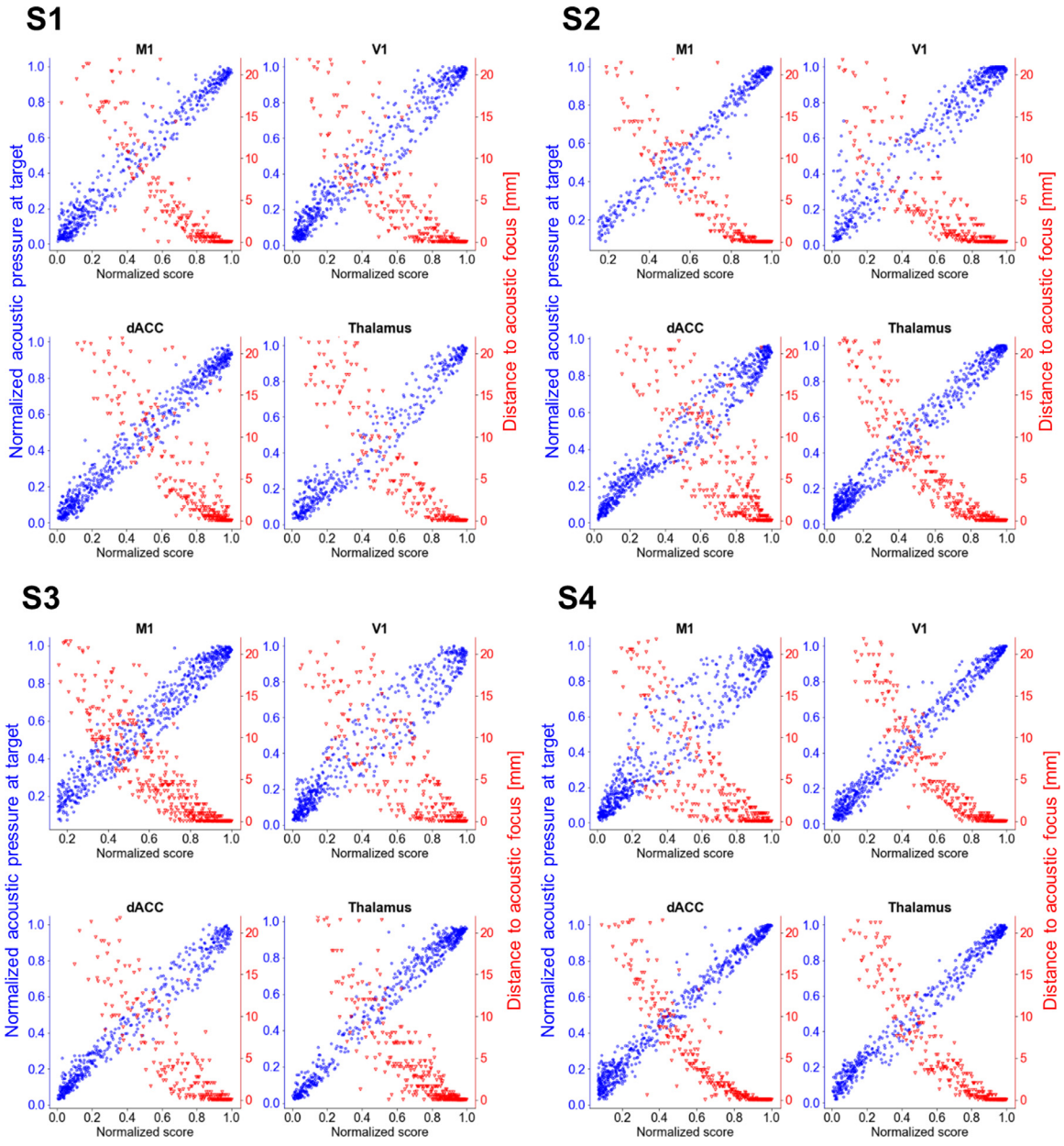

Fig. 5. Simulated results at a given score when the targeting M1, V1, dACC, and thalamus. Blue circles indicate P_{target}. Red triangles represented Δd.

2.7. Experimental validation

Experimental validation using the ex vivo human skull was also performed. The optimized transducer location was determined using the proposed method to target the dACC region in the brain. The target coordinates of the dACC were chosen based on the ICBM152 template. A 3D-printed skull guide, as shown in Fig. 3a, was used to accurately locate the optimized transducer location [25]. The measurement setup is shown in Fig. 3b. The single-element transducer was driven by a power amplifier (240 L, Electronics & Innovations Ltd., Rochester, NY) and a function generator (Agilent 33210A, Keysight Technologies Inc., USA). The driving input signal was the pulsed sinusoidal waves with a fundamental frequency of 250 kHz, tone burst duration of 100 μs, and duty cycle of 3%. A needle-type hydrophone (HNR500, Onda, Sunnyvale, CA) was used to measure the transcranial 3D acoustic pressure field. The hydrophone was controlled using a three-axis positioning system (Bi-Slide Velmex, Inc. Bloomfield, NY) with a 0.5 mm step size. To obtain the locations of the hydrophone relative to the skull and transducer, an image-guided navigation system with an optical camera (Polaris Vicra, NDI, Waterloo, ON, Canada) was implemented in SlicerIGT [40] (Fig. 3b). The rigid body trackers were attached to the 3D-printed guide and positioning system (Fig. 3b). Using the measured intracranial pressure field, the spatial conformity of the acoustic focus was assessed by P_{target} and Δd mentioned above.

In addition, the measured pressure distribution was compared with the pressure distribution obtained from the forward simulation. Both the measured and simulated pressure distributions were normalized with respect to the measured peak intracranial pressure ($\bar{P}_{peak}$). The accuracy of the simulation was quantified in terms of the target pressure ratio (Δ_{Target}), peak intracranial pressure ratio (Δ_{PR}), and dice similarity coefficient of acoustic focus ($DSC_{A90\%}$)

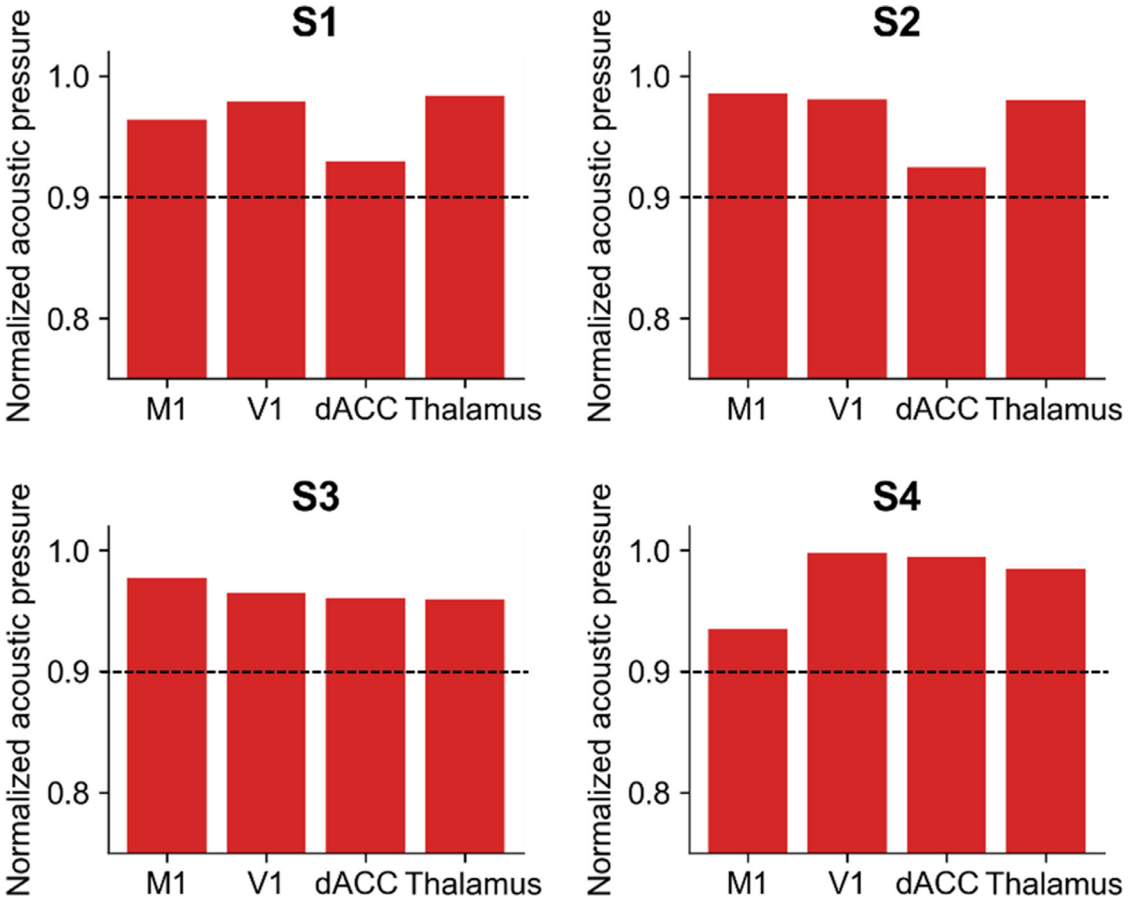

Fig. 6. P_{target} at the optimal transducer location for all brain targets across all subjects.

[28] as follows:

$$\Delta_{Target} = \frac{\left|P_{target} - \bar{P}_{target}\right|}{\bar{P}_{target}}, \ \Delta_{PR} = \frac{\left|P_{peak} - \bar{P}_{peak}\right|}{\bar{P}_{peak}}, \text{ and } DSC_{A90\%} = \frac{2\left(A_{90\%} \cap \bar{A}_{90\%}\right)}{A_{90\%} + \bar{A}_{90\%}} \quad (15)$$

where the quantity with an upper bar indicates the measurement, and the others are simulated.

3. Result

3.1. Numerical validation

Fig. 4 shows an example of the 3D acoustic pressure distribution and $A_{90\%}$ from the forward simulation depending on the score of the transducer location with the dACC region in S3 as the target. The scores were normalized with respect to the maximum score value. The target was located inside the $A_{90\%}$ when the score was maximum (i.e., 1), whereas the target was outside the $A_{90\%}$ when the score was relatively low (i.e., 0.2 and 0.5).

Fig. 5 shows the relationship between the score value for each transducer location and the corresponding P_{target} and Δd. In all brain targets (M1, V1, dACC, and thalamus) across all subjects (n = 4), the score showed a linear relationship with P_{target} and an inverse relationship with Δd. Fig. 6 represents P_{target} at the optimal transducer location (i.e., in the case of the maximum score value). that indicates over 0.9 (i.e., $\Delta d = 0$) for all cases.

3.2. Experimental validation

Fig. 7 shows the acoustic pressure distribution at the optimized transducer location obtained from the forward simulation and the actual measurement using an *ex vivo* human skull. From the measurement result, $\bar{P}_{target}$ (measured pressure at the target point) was 0.93, and the target was located within $\bar{A}_{90\%}$.

The simulated pressure profile also indicated that the target coordinates were within $A_{90\%}$, and P_{target} was 0.94. The simulated and measured pressure distributions, Δ_{Target}, Δ_{PR}, and $DSC_{A90\%}$ were 1%, 6.8%, and 0.40, respectively.

4. Discussion

In the present study, we propose a method that finds the optimal location of a single-element FUS transducer for accurate targeting of a region inside the brain. The score function (ψ) representing the superposition of ultrasound waves according to the phase difference ($\Delta\varphi_{i,j,k}$) and pressure transmissibility ($A_{i,j,k}$) was calculated depending on the spatial location of the transducer. The optimized transducer location, having the maximum score value, was then determined using the DE method. From the numerical results presented in Figs. 4 and 5, the score value showed a positive proportional relationship with P_{target}. For the optimal transducer location, $P_{target} > 0.9$ and $\Delta d = 0$ were achieved in all cases. Similar to the numerical results, the experimental validation results indicated that the target was located within $\bar{A}_{90\%}$ (i.e., $\Delta d = 0$) and $\bar{P}_{target}$ was 0.93. These results demonstrate that the optimal location of the transducer predetermined by the proposed method

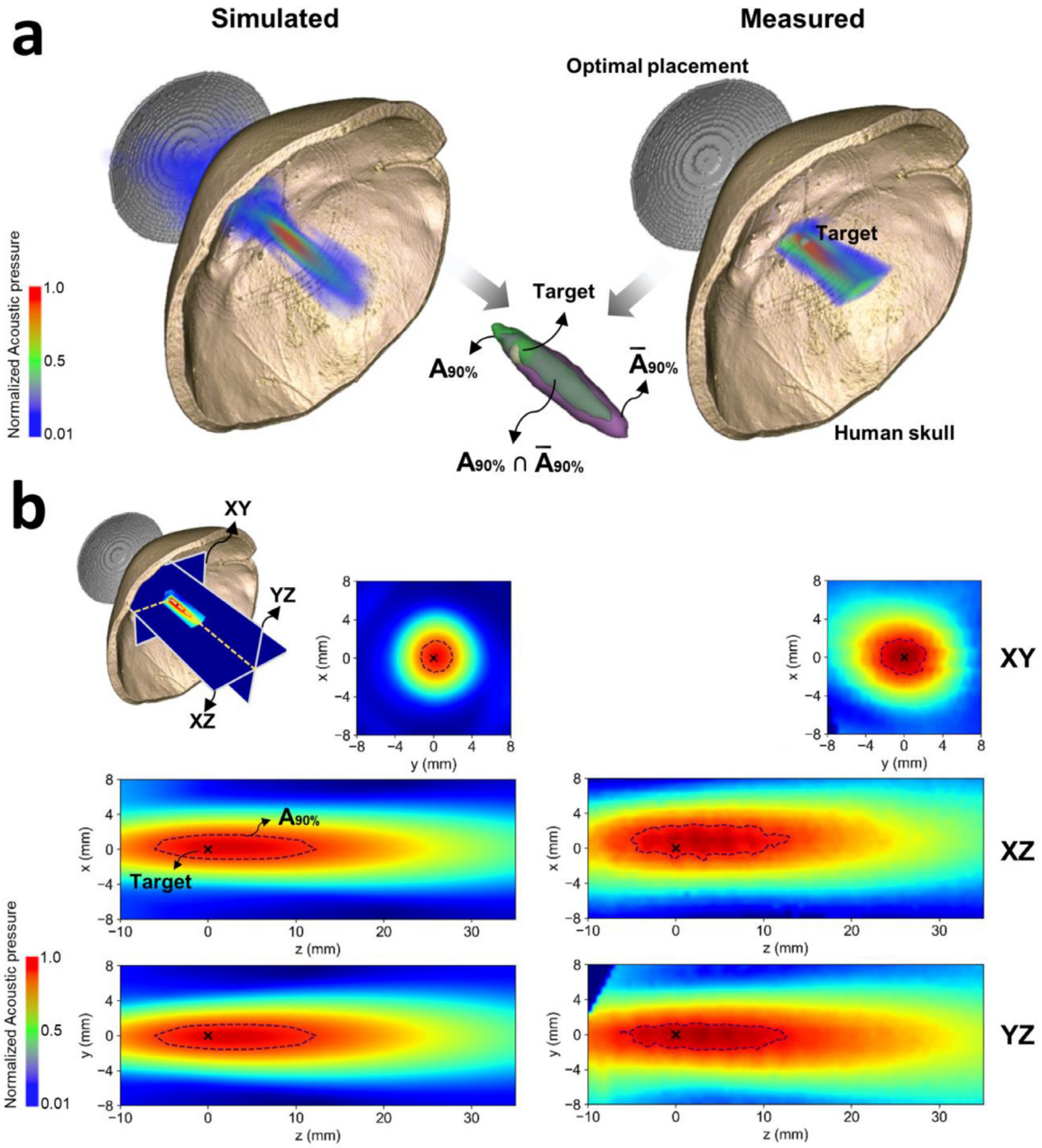

Fig. 7. Simulated (left column) and measured (right column) results at the optimal transducer's location in the *ex vivo* human skull. (a) 3D acoustic pressure distribution and $A_{90\%}$. (b) 2D acoustic pressure profiles at the perpendicular planes intersecting the target point. The 'x' mark and dashed lines indicate the target point and $A_{90\%}$ of acoustic pressure, respectively.

can be used for transcranial FUS treatment planning in conjunction with a conventional image-guided navigation system [17,22,41] and the 3D printed mask system [20].

Similar to our work, Park et al. proposed a method that finds the optimal position of a single-element transducer by calculating the reflection coefficient between the skull and transducer [25]. The reflection coefficient was obtained at each possible position of the transducer, and the position with the lowest reflection coefficient was selected as the optimal position. However, this method, which simplified the ultrasonic wave as straight lines, could not fully describe the wave propagation through the skull and was therefore limited to targeting only specific brain regions. The method was only validated when targeting the cortical region of the brain. The method proposed herein addresses this limitation by using the time-reversal simulation, showing reliable results in various brain regions (cortical: M1, V1; subcortical: dACC; deep brain: thalamus). In addition, although the previous method could determine the optimal transducer position, the orientation of the transducer was not optimized. However, the present work is expected to yield better results by optimizing both the position and orientation of the transducer.

In this study, the DE method was used to optimize the spatial location of the transducer. Conventional gradient-based optimization methods, such as gradient descent and quasi-Newton, are prone to converge to local minima generated by the undulating form of the phase profile [42]. In contrast, the DE method optimizes a problem by iteratively improving a candidate solution without using a gradient [31,42]. Moreover, the metaheuristic approach of DE makes it possible to search a relatively large space of candidate solutions; therefore, Ω_m can be defined as a 3D vol-

ume rather than a 2D surface, and the orientation of the transducer could also be optimized [43]. The numerical and experimental results (Fig. 6 and 7) indicate that DE is a suitable method for our optimization problem (p), Eq. 8. Although DE shows promising results in our study, it is still possible that a globally optimal solution may not be reached [32]. The controllable parameters of DE, such as the crossover probability, scaling factor, and population size, should be adjusted for better performance in future studies [32,44].

The score function based on the time-invariance of the acoustic wave was significantly affected by the accuracy of the acoustic simulation. Therefore, to evaluate the accuracy of the acoustic simulation, the simulated and measured acoustic pressure distributions were compared. Unlike previous studies that measured the acoustic field only in the 2D plane [35,45], the actual 3D acoustic pressure distribution was obtained for a more precise evaluation. Importantly, Δ_{Target} and Δ_{PR} were 1% and 6.8%, respectively, indicating that the accuracy of the acoustic simulation used in this study is comparable to that of a previous study [35]. Moreover, $DSC_{A90\%}$ (=0.4), which is a measure of the spatial similarity of two 3D acoustic foci (see Fig. 7a), also indicates an acceptable level for practical applications. Although our numerical model showed promising accuracy relative to actual measurements, it would be interesting to consider the nonlinearity of wave propagation and shear mode conversion for better acoustic simulation accuracy.

In this study, we used only a 250 kHz FUS transducer with a diameter of 95 mm and ROC of 99 mm, which means that our validation results were limited to the specific geometry of the transducer. Because the proposed score function ($\psi(\mathbf{D}(\mathbf{X}))$) is affected by the discretized shape of the transducer ($\mathbf{D}(\mathbf{X})$), the proposed method needs to be validated with varying transducer geometry. Moreover, various modeling methods to discretize the transducers [45] can be applied to improve the score function. Another limitation of this study is that an investigation into the influence of driving frequency was not considered. Because the accuracy of the acoustic simulation decreases with increasing driving frequency, the accuracy of the proposed method based on time-reversal simulation could be significantly affected by varying the driving frequency. Therefore, it would be interesting to study the effect of change in the driving frequency on the proposed method in the future. Finally, the requirement of a target into the brain is also a significant issue for time-reversal simulations/measurements. The target characteristics (e.g., shape, size, and composition) that affect the time-reversal operator should be investigated in future work [46].

5. Conclusion

In this study, we developed an optimization method to find the optimal location of a single-element transducer that effectively transmits acoustic energy to a target in the brain. First, the score function representing the superposition of ultrasound waves based on the time-reversal simulation was calculated for a given transducer location. Then, the optimal transducer location, having the maximum score, was found using the DE algorithm. Numerical and experimental validations were performed with the acoustic simulations and the ex vivo human skull, respectively. The results indicated that the score had a positive proportional relationship with the acoustic pressure at the target. Moreover, when the transducer location was optimized using the proposed method, the normalized acoustic pressure at the target point was higher than 0.9, and the distance (Δd) between the target and $A_{90\%}$ was 0 in all cases. The results demonstrate that the proposed method can be successfully used to determine the optimal location of a single-element FUS transducer for accurate targeting.

Declaration of Competing Interest

The authors declare that they have no known competing financial interests or personal relationships that could have appeared to influence the work reported in this paper.

Acknowledgment

This work was supported by the Korea Institute of Science and Technology (KIST) Institutional Program (No. 2E31071) and the National Research Council of Science and Technology (NST) grant by the Korean government (MSIT) (No. CAP-18014-000).

References

[1] H Baek, KJ Pahk, H. Kim, A review of low-intensity focused ultrasound for neuromodulation, Biomed Eng Lett 7 (2017) 135–142, doi:10.1007/s13534-016-0007-y.
[2] C Pasquinelli, LG Hanson, HR Siebner, HJ Lee, A. Thielscher, Safety of transcranial focused ultrasound stimulation: A systematic review of the state of knowledge from both human and animal studies, Brain Stimul 12 (2019) 1367–1380, doi:10.1016/j.brs.2019.07.024.
[3] W Legon, S Adams, P Bansal, PD Patel, L Hobbs, L Ai, et al., A retrospective qualitative report of symptoms and safety from transcranial focused ultrasound for neuromodulation in humans, Sci Rep 10 (2020) 1–10, doi:10.1038/s41598-020-62265-8.
[4] A Fomenko, C Neudorfer, RF Dallapiazza, SK Kalia, AM. Lozano, Low-intensity ultrasound neuromodulation: An overview of mechanisms and emerging human applications, Brain Stimul 11 (2018) 1209–1217, doi:10.1016/j.brs.2018.08.013.
[5] JK Mueller, L Ai, P Bansal, W. Legon, Numerical evaluation of the skull for human neuromodulation with transcranial focused ultrasound, J Neural Eng 14 (2017) 066012, doi:10.1088/1741-2552/aa843e.
[6] A Kyriakou, E Neufeld, B Werner, MM Paulides, G Szekely, N Kuster, et al., A review of numerical and experimental compensation techniques for skull-induced phase aberrations in transcranial focused ultrasound, Int J Hyperth 30 (2014) 36–46, doi:10.3109/02656736.2013.861519.
[7] SA Leung, D Moore, TD Webb, J Snell, P Ghanouni, K. Butts Pauly, Transcranial focused ultrasound phase correction using the hybrid angular spectrum method, Sci Rep 11 (2021) 1–14, doi:10.1038/s41598-021-85535-5.
[8] JL Thomas, MA. Fink, Ultrasonic beam focusing through tissue inhomogeneities with a time reversal mirror: application to transskull therapy, IEEE Trans Ultrason Ferroelectr Freq Control 43 (1996) 1122–1129, doi:10.1109/58.542055.
[9] M. Fink, Time-reversal acoustics, J Phys Conf Ser 118 (2008), doi:10.1088/1742-6596/118/1/012001.
[10] Y Jing, FC Meral, GT. Clement, Time-reversal transcranial ultrasound beam focusing using a k-space method, Phys Med Biol 57 (2012) 901–917, doi:10.1088/0031-9155/57/4/901.
[11] D Coluccia, J Fandino, L Schwyzer, R O'Gorman, L Remonda, J Anon, et al., First noninvasive thermal ablation of a brain tumor with MR-guided focused ultrasound, J Ther Ultrasound 2 (2014) 1–7, doi:10.1186/2050-5736-2-17.
[12] U Vyas, E Kaye, KB. Pauly, Transcranial phase aberration correction using beam simulations and MR-ARFI, Med Phys 41 (2014) 1–10, doi:10.1118/1.4865778.
[13] M Aryal, CD Arvanitis, PM Alexander, N. McDannold, Ultrasound-mediated blood-brain barrier disruption for targeted drug delivery in the central nervous system, Adv Drug Deliv Rev 72 (2014) 94–109, doi:10.1016/j.addr.2014.01.008.
[14] Smirnov P, Hynynen K, Jones RM, Hynynen K, Bouchoux G, Bader KB, et al. The design of a focused ultrasound transducer array for the treatment of stroke : a simulation study The design of a focused ultrasound transducer array for the treatment of stroke : a simulation study n.d. https://doi.org/ 10.1088/0031-9155/57/15/4951.
[15] D Jeanmonod, B Werner, A Morel, L Michels, E Zadicario, G Schiff, et al., Transcranial magnetic resonance imaging-guided focused ultrasound: noninvasive central lateral thalamotomy for chronic neuropathic pain, Neurosurg Focus 32 (2012) 1–11, doi:10.3171/2011.10.FOCUS11248.
[16] BW Badran, KA Caulfield, S Stomberg-Firestein, PM Summers, LT Dowdle, M Savoca, et al., Sonication of the anterior thalamus with MRI-Guided transcranial focused ultrasound (tFUS) alters pain thresholds in healthy adults: A double-blind, sham-controlled study, Brain Stimul 13 (2020) 1805–1812, doi:10.1016/j.brs.2020.10.007.
[17] W Lee, DS Weisholtz, GE Strangman, S-S. Yoo, Safety Review and Perspectives of Transcranial Focused Ultrasound Brain Stimulation, Brain & Neurorehabilitation 14 (2021), doi:10.12786/bn.2021.14.e4.
[18] S-S. Yoo, Technical Review and Perspectives of Transcranial Focused Ultrasound Brain Stimulation for Neurorehabilitation, Brain & Neurorehabilitation 11 (2018), doi:10.12786/bn.2018.11.e16.
[19] S Kim, Y Jo, G Kook, C Pasquinelli, H Kim, K Kim, et al., Transcranial focused ultrasound stimulation with high spatial resolution, Brain Stimul 14 (2021) 290–300, doi:10.1016/j.brs.2021.01.002.
[20] H Joe, KJ Pahk, S Park, H. Kim, Development of a Subject-specific Guide System for Low-Intensity Focused Ultrasound (LIFU) Brain Stimulation, Comput Methods Programs Biomed 176 (2019) 105–110, doi:10.1016/j.cmpb.2019.05.001.

[21] W Lee, YA Chung, Y Jung, I-U Song, S-S. Yoo, Simultaneous acoustic stimulation of human primary and secondary somatosensory cortices using transcranial focused ultrasound, BMC Neurosci 17 (2016) 17–68, doi:10.1186/s12868-016-0303-6.
[22] W Lee, SD Lee, MY Park, L Foley, E Purcell-Estabrook, H Kim, et al., Image-Guided Focused Ultrasound-Mediated Regional Brain Stimulation in Sheep, Ultrasound Med Biol 42 (2016) 459–470, doi:10.1016/j.ultrasmedbio.2015.10.001.
[23] S Jiménez-Gambín, N Jiménez, JM Benlloch, F. Camarena, Holograms to Focus Arbitrary Ultrasonic Fields through the Skull, Phys Rev Appl 12 (2019), doi:10.1103/physrevapplied.12.014016.
[24] M Ferri, JM Bravo, J Redondo, J V Sánchez-Pérez, Enhanced Numerical Method for the Design of 3-D-Printed Holographic Acoustic Lenses for Aberration Correction of Single-Element Transcranial Focused Ultrasound, Ultrasound Med Biol 45 (2019) 867–884, doi:10.1016/j.ultrasmedbio.2018.10.022.
[25] TY Park, KJ Pahk, H. Kim, Method to optimize the placement of a single-element transducer for transcranial focused ultrasound, Comput Methods Programs Biomed 179 (2019) 104982, doi:10.1016/j.cmpb.2019.104982.
[26] BE Treeby, BT. Cox, k Wave, MATLAB toolbox for the simulation and reconstruction of photoacoustic wave fields, J Biomed Opt 15 (2010) 021314, doi:10.1117/1.3360308.
[27] R Beare, B Lowekamp, Z. Yaniv, Image segmentation, registration and characterization in R with simpleITK, J Stat Softw 86 (2018), doi:10.18637/jss.v086.i08.
[28] Koh H, Park TY, Chung YA, Lee J, Kim H. Acoustic simulation for transcranial focused ultrasound using GAN-based synthetic CT 2021;2194:1–11. https://doi.org/ 10.1109/JBHI.2021.3103387.
[29] H Jeong, JJ Im, JS Park, SH Na, W Lee, SS Yoo, et al., A pilot clinical study of low-intensity transcranial focused ultrasound in alzheimer's disease, Ultrasonography 40 (2021) 512–519, doi:10.14366/USG.20138.
[30] Jeong H, Song I, Chung Y, Park J, Na S, Im JJ, et al. Short-Term Efficacy of Transcranial Focused Ultrasound to the Hippocampus in Alzheimer ' s Disease : A Preliminary Study 2022.
[31] H Li, PGH Nichols, S Han, KJ Foster, K Sivasithamparam, MJ. Barbetti, Differential Evolution – A Simple and Efficient Heuristic for Global Optimization over Continuous Spaces, J OfGlobal Optim (1997) 341–359, doi:10.1071/AP09004.
[32] AW Mohamed, HZ Sabry, M. Khorshid, An alternative differential evolution algorithm for global optimization, J Adv Res 3 (2012) 149–165, doi:10.1016/j.jare.2011.06.004.
[33] Eric Jones, Travis Oliphant PP, others. SciPy, Open Source Scientific Tools for Python (2001) http://www.scipy.org.
[34] F Yates, D Sc, RE. Station, Systematic Sampling, Philos Trans R Soc a Mathmetical 241 (1948) 346–377, doi:10.1002/9780470374597.ch4.
[35] K Yoon, W Lee, P Croce, A Cammalleri, S-S. Yoo, Multi-resolution simulation of focused ultrasound propagation through ovine skull from a single-element transducer, Phys Med Biol 63 (2018) 105001, doi:10.1088/1361-6560/aabe37.
[36] H Kim, SD Lee, A Chiu, SS Yoo, S. Park, Estimation of the spatial profile of neuromodulation and the temporal latency in motor responses induced by focused ultrasound brain stimulation, Neuroreport 25 (2014) 475–479, doi:10.1097/WNR.0000000000000118.
[37] H Kim, MA Park, S Wang, A Chiu, K Fischer, SS. Yoo, PET/CT imaging evidence of FUS-mediated (18)F-FDG uptake changes in rat brain, Med Phys 40 (2013) 1–10, doi:10.1118/1.4789916.
[38] V Fonov, AC Evans, K Botteron, CR Almli, RC McKinstry, DL. Collins, Unbiased average age-appropriate atlases for pediatric studies, Neuroimage 54 (2011) 313–327, doi:10.1016/j.neuroimage.2010.07.033.
[39] S Klein, M Staring, K Murphy, M a Viergever, J.elastix Pluim, A Toolbox for Intensity-Based Medical Image Registration, IEEE Trans Med Imaging 29 (2010) 196–205.
[40] T Ungi, A Lasso, G. Fichtinger, Open-source platforms for navigated image-guided interventions, Med Image Anal 33 (2016) 181–186, doi:10.1016/j.media.2016.06.011.
[41] W Lee, HC Kim, Y Jung, YA Chung, IU Song, JH Lee, et al., Transcranial focused ultrasound stimulation of human primary visual cortex, Sci Rep 6 (2016) 34026–34037, doi:10.1038/srep34026.
[42] A. Qing, Comment on "differential Evolution as Applied to Electromagnetics, IEEE Antennas Propag Mag 53 (2011) 169–171, doi:10.1109/MAP.2011.6097316.
[43] Melo VV De, Delbem AC Botazzo, Investigating Smart Sampling as a population initialization method for Differential Evolution in continuous problems, Inf Sci (Ny) 193 (2012) 36–53, doi:10.1016/j.ins.2011.12.037.
[44] T Eltaeib, A. Mahmood, Differential evolution: A survey and analysis, Appl Sci 8 (2018), doi:10.3390/app8101945.
[45] C Pasquinelli, H Montanaro, HJ Lee, LG Hanson, H Kim, N Kuster, et al., Transducer modeling for accurate acoustic simulations of transcranial focused ultrasound stimulation, J Neural Eng 17 (2020), doi:10.1088/1741-2552/ab98dc.
[46] DH Chambers, L. Livermore, Target characterization using time-reversal symmetry of wave propagation 21 (2007) 3511–3555.